

BeppoSAX observation of NGC3923, and the problem of the X-ray emission in E/S0 galaxies of low and medium L_X/L_B

S. Pellegrini

Dipartimento di Astronomia, Università di Bologna, via Zamboni 33, I-40126 Bologna
email: pellegrini@astbo3.bo.astro.it

Received...; accepted ...

Abstract. We present the results of the analysis of the *BeppoSAX* LECS and MECS pointed observation of the E4 galaxy NGC 3923, for which previous X-ray measurements had given a medium X-ray to optical ratio L_X/L_B . The spectral analysis over (0.5–10) keV reveals that the best representation of the data is the superposition of two thermal components at temperatures of 0.4 keV and 6–8 keV. The total emission is roughly equally divided between the two components, over (0.5–4.5) keV. Abundances are very subsolar at the best fit, but not constrained by the data. The harder component is consistent with an origin from stellar sources; the softer component likely comes from hot gas. L_X of this hot gas is not as large as expected for a global inflow, in a galaxy of an optical luminosity as high as that of NGC 3923. So, it is suggested that a substantial amount of hot gas was removed by internal agents, and that this process was helped by the flat mass distribution of the galaxy. Another possibility is that gas was lost as a consequence of the episod of interaction or merger that produced the system of shells visible in the optical band. Finally, the possible origins of the large scatter in the X-ray emission shown by galaxies of similar L_B are also reviewed. Like NGC 3923, many other low and medium L_X/L_B galaxies reside in small groups, in which the ambient medium (if present) cannot strip them of their hot gas; so, if only environmental factors are invoked to lower L_X/L_B , the most effective mechanism must be galaxy interactions. The lower L_X/L_B galaxies, though, are seen to occur across the whole range of galaxy densities. Another possibility, to remove some or all of the hot gas, appeals to mechanisms internal to the galaxies, such as heating of the gas by supernovae explosions or accretion onto central massive black holes. This has been shown to work in general, for a large range of L_B , but it is not clear yet whether the hot gas abundances estimated from recent observations can be accommodated in it.

Key words: Galaxies: elliptical and lenticular, cD - Galaxies: individual: NGC 3923 - Galaxies: ISM - X-rays: galaxies - Radiation mechanisms: miscellaneous

1. Introduction

X-ray observations, beginning with the *Einstein* Observatory (Giacconi et al. 1979), have demonstrated that normal early-type galaxies are X-ray emitters, with 0.2–4 keV luminosities ranging from $\sim 10^{40}$ to $\sim 10^{43}$ erg s $^{-1}$ (Fabbiano 1989; Fabbiano et al. 1992). The X-ray luminosity L_X is found to correlate with the blue luminosity L_B ($L_X \propto L_B^{2.0 \pm 0.2}$), but there is a large scatter of roughly two orders of magnitude in L_X at any fixed $L_B > 3 \times 10^{10} L_\odot$. The analysis of the *Einstein* spectral data already revealed that in the X-ray brightest objects the X-ray radiation comes from thermal emission from a hot, optically thin gas, at a temperature of ~ 1 keV (Canizares et al. 1987, hereafter CFT). It also revealed that the X-ray emission temperature increases with decreasing L_X/L_B , until the dominant contribution to the total emission comes from a hard thermal component, similar to that dominating the emission in spiral galaxies (Kim et al. 1992). Since a population of low mass X-ray binaries (LMXB) can explain the X-ray emission of the bulge of M31, and that of bulge-dominated spirals, it is likely that in early-type galaxies an increasing fraction of the X-ray emission comes from stellar sources as L_X/L_B decreases. Better quality spectra of low and medium L_X/L_B galaxies (i.e., belonging to Group 1 or Group 2 in the analysis of Kim et al. 1992, or with $L_X/L_B < 30.3$ in the *Einstein* band) have been made available recently for several galaxies, thanks to *ROSAT* and *ASCA* pointed observations.

The analysis of *ROSAT* data confirmed the findings based on the *Einstein* data for several low and medium L_X/L_B galaxies (see, e.g., the sample of 61 early-type galaxies observed with the *ROSAT* PSPC built by Irwin & Sarazin 1998). The emerging picture was the existence of at least two spectral components, a soft one likely due to hot gas or stellar sources, and a hard one, whose temperature is not well constrained, due to the lack of sensitivity of the PSPC above 2 keV.

Sensitive over (0.5–10) keV, *ASCA* pointed ~ 30 early-type galaxies, among which there are a handful with low or medium L_X/L_B (Matsushita et al. 1994; Kim et al. 1996; Matsumoto et al. 1998; Buote & Fabian 1998, hereafter BF). In all the 12 E/S0s of their sample Matsumoto et al. find a variable amount of soft thermal emission, of temperature ranging from 0.3 to 1 keV, coupled to hard emission. The amount of this hard emission roughly scales as the optical luminosity of the galaxies, and is consistent with that of bulge-dominated spirals, such as M31. Using *ASCA* data over the energy range 0.5–5 keV, also BF find a hard component of $kT > 2$ keV coupled with a soft component, in the low or medium L_X/L_B galaxies of their sample.

The precise knowledge of the contribution of stellar sources to the total X-ray emission is important to better constrain the properties of the hot gas (i.e., temperature, abundance and luminosity), or to identify peculiarities such as the presence of a mini-AGN, another possible contributor to the hard emission (e.g., Colbert & Mushotzky 1998). So, stronger constraints on the gas flow phase and the galaxy properties can be derived. The contribution of stellar sources can be best evaluated with observations over a large bandwidth. In this paper we report on the X-ray emission from the E4 galaxy NGC 3923, as detected by the *BeppoSAX* satellite over (0.5–10) keV. Our purpose is to investigate in detail the nature of the X-ray emission in this medium L_X/L_B galaxy (*Einstein* observations showed that $\log(L_X/L_B) = 30.24$ for it, Fabbiano et al. 1992). The *BeppoSAX* observation of NGC 3923, exploiting a moderate spatial resolution coupled with the large energy band and the good spectral resolution of the satellite, permits the separation of the soft and the hard emission components eventually present. The spectral properties of NGC 3923 over 0.5–5 keV have been already studied by BF, using *ASCA* data referring to a radius of 2 arcmin (note that the radius encircling 80% of the photons of a point source is 3 arcmin for the *ASCA*-XRT). The *BeppoSAX* observation of NGC 3923 presents some advantages over that performed by *ASCA*: a sharper PSF above 2 keV with respect to that of the *ASCA*-XRT, which is also asymmetrical¹; a lower instrumental background for the MECS with respect to the GIS, which favors weak sources. Finally, a larger covering in energy is presented here with respect to that analysed by BF (i.e., 0.5–10 keV versus 0.5–5 keV), a spatial analysis is attempted over (1.7–10) keV, and a larger extraction region for the spectral data is used. NGC 3923 has been pointed also by the *ROSAT* PSPC and HRI, which allowed a detailed inves-

tigation of the spatial distribution of the X-ray emission (Buote Canizares 1998, hereafter BC).

This paper is organized as follows: we present in Sect. 2 the main properties of NGC 3923, in Sect. 3 the results of the data analysis, in Sect. 4 the possible origins for the X-ray emissions of NGC 3923 are discussed in light of the present results, and more in general the possible origins of the large scatter in the X-ray emission shown by galaxies of similar L_B are also reviewed; in Sect. 5 we summarize the conclusions.

2. General characteristics of NGC 3923

The main characteristics of NGC 3923 are summarized in Table 1. This is the dominant galaxy of a small group of five objects (LGG255, Garcia 1993); the other members are one elliptical (NGC 3904), one lenticular and two spirals. The velocity dispersion of the group is 184 km s^{-1} (Huchra & Geller 1982). No extended X-ray emission has been detected other than that associated with the galaxy, from a possible intragroup medium (Forman et al. 1985). NGC 3923 is one of the best known examples of an elliptical galaxy with shells (e.g., Carter et al. 1998). In NGC 3923 the shells are expected to be the result of two possible processes: a low-velocity merger with a less massive galaxy which is eventually disrupted, on a long time scale of several Gyrs (Quinn 1984); or a weak interaction, which took place a couple of Gyrs ago, with a passing galaxy of much smaller mass (Thomson 1991). NGC 3923 shows no rotation on its major axis (e.g., Pellegrini et al. 1997), and small minor axis rotation (Carter et al. 1998), which is consistent with either the presence of a kinematically decoupled core, established during a merger, or triaxiality (Franx et al. 1989). The modest content of cold gas and dust in NGC 3923 is consistent with a merger with a dwarf spheroidal; this would also explain the absence of radio activity, or of enhanced star formation (Forbes 1991). In case, any enhanced activity is expected to have occurred on a shorter time-scale than that of the long-lived shells. In all other respects except the presence of shells, NGC 3923 appears to be an ordinary elliptical galaxy, whose projected image on the sky is quite flat.

3. X-ray Data Analysis

NGC 3923 was observed by two Narrow Field Instruments on board the *BeppoSAX* satellite (Boella et al. 1997a): the Low Energy Concentrator Spectrometer (LECS) and the Medium Energy Concentrator Spectrometer (MECS). The journal of the observation is given in Table 2. LECS and MECS are made of grazing incidence telescopes with position sensitive gas scintillation proportional counters in their focal planes. The MECS, which consists of three equal units, has a field of view of 56 arcmin diameter, works in the range 1.5–10 keV, with an energy resolution of $\sim 8\%$, and moderate spatial resolution of ~ 0.7 arcmin

¹ For example, the half power radius measured for the on-axis PSF at 6 keV is about a factor of two smaller than that of the *ASCA* on-axis PSF; the comparison is even more favorable at the 80% and 90% radii, due to the considerably reduced scattering of the MECS optics (Boella et al. 1997b).

Table 1. General characteristics of NGC 3923

Type ^a	RA (J2000)	Dec (J2000)	PA ^a (deg)	d ^b (Mpc)	B_T^0 ^a (mag)	$\log L_B$ ^c (L_\odot)	R_e ^a	b/a ^a	σ ^d (km s ⁻¹)	N_H ^e (cm ⁻²)
E4	11 ^h 51 ^m 02 ^s .1	-28°48'23''	50	41.5	10.27	11.3	49'8	0.66	241	6.4×10^{20}

^a from de Vaucouleurs et al. 1991. PA is the position angle of the optical major axis; B_T^0 is the total B magnitude, corrected for galactic and internal extinction; R_e is the effective radius, and b/a is the minor to major axes ratio.

^b distance from Fabbiano et al. (1992), who adopt a Hubble constant of 50 km s⁻¹ Mpc⁻¹.

^c total B-band luminosity L_B , derived using the indicated distance and B_T^0 .

^d central stellar velocity dispersion from McElroy (1995).

^e Galactic neutral hydrogen column density from Stark et al. (1992).

FWHM at 6 keV (Boella et al. 1997b). The total effective area of the MECS is comparable to that of the 2 GIS units on board *ASCA*. The LECS is sensitive also at softer energies (over 0.5–10 keV), has a field of view of 37 arcmin diameter, an energy resolution a factor of ~ 2.4 better than that of the *ROSAT* PSPC, but an effective area much lower (between a factor of 6 and 2 lower, going from 0.3 to 1.5 keV; Parmar et al. 1997).

The cleaned and linearized data have been retrieved from the *BeppoSAX* Science Data Center archive, and later reduced and analysed using the standard software (XSELECT v1.3, FTOOLS v4.0, IRAF-PROS v2.5, and XSPEC v10.0). For the MECS, the event file made by merging the data of the 3 MECS units, properly equalized, has been used.

3.1. Spatial Analysis

In Fig. 1 a contour plot of the MECS image is shown. The counts in this image belong to pulse invariant gain-corrected spectral channels 29–218 (~ 1.7 –10 keV). The data have been smoothed with a gaussian of $\sigma = 1'$. An extended source is clearly visible, of extension larger than the PSF, and covering at least 8 optical effective radii. The X-ray emission shows roughly the same position angle of the optical emission. The background subtracted radial profile obtained from the MECS data over 1.7–10 keV is plotted in Fig. 2.

The X-ray source extent needs to be estimated precisely, in order to determine the size of the region from which to extract the counts for the spectral analysis, and the estimate of the flux. We consider the source boundary to be the point at which the total (i.e., source+background) X-ray surface brightness flattens onto the background level. The background is estimated from blank fields event files², accumulated on five

different pointings of empty fields, and using extraction regions corresponding in size and position to those of the source. In addition to the inspection of various surface brightness profiles (e.g., the azimuthally averaged one, and also those along the major and minor axes), the precise source extent was finally established also through the requirement that within it the S/N of the background-subtracted counts keeps at a high value, not much lower than that of the central regions of the galaxy. This produced an extraction region of an ellipse for the MECS data, of semimajor axis of 8' and semiminor axis of 6' (Table 2). The PSF of the LECS is a strong function of energy, and it is broader than that of the MECS below 1 keV, while it is similar to that of the MECS above 2 keV. A radius of 8' is suggested to encircle all the photons of soft sources (<http://www.sdc.asi.it/software/cookbook>). This radius turned out to be optimal in our case, satisfying both the requirement of being the radius at which the brightness profile flattens onto the background level, and that of a high S/N. These different extraction regions for the LECS and the MECS images encircle the same fraction of the source photons, in a given band common to the two instruments, as verified later during the spectral analysis.

Analyzing the *ROSAT* PSPC image of NGC 3923, BC detected a few foreground/background sources; those falling within the extraction region are displayed in Fig. 1. The nature of these sources is unknown. Sources called "1", "NWa", and "NWb" by BC cannot be distinguished in the MECS image, while this image looks quite aligned to the North-South due to source "2". By deriving the net counts in each one of four quadrants, obtained by dividing the extraction region ellipse with its major and minor axes, it turns out that the quadrant comprising sources "1", "2", and "NWb" has roughly 60 ± 20 net counts more than the average of the others. This is a contribution of $\sim 14\%$ to the MECS net counts. The quadrant with source "NWa" shows no significant net counts enhancement. By inspecting the surface brightness profile in a stripe across source "2", a contribution of ~ 16 net counts is estimated from this source; this is likely to be responsible for the jump at a radius of 260'' in the azimuthally averaged

² This choice was motivated by the fact that at radii $> 10'$ the energy dependent vignetting of the mirrors is not negligible. In the position of the galaxy instead, i.e., on-axis within radii of 10', the vignetting effect is negligible, well within the uncertainties in the profile.

Fig. 1. The MECS image of NGC 3923, smoothed with a gaussian of $\sigma = 1'$. Contours plotted correspond 27, 30, 33, 39, 45, 55, 70, 85, 95 % of the peak intensity. The numbers 1, 2, 3, 4 mark respectively the positions of the foreground/background sources 1, 2, NWa and MWb found by BC in the *ROSAT* image of NGC 3923.

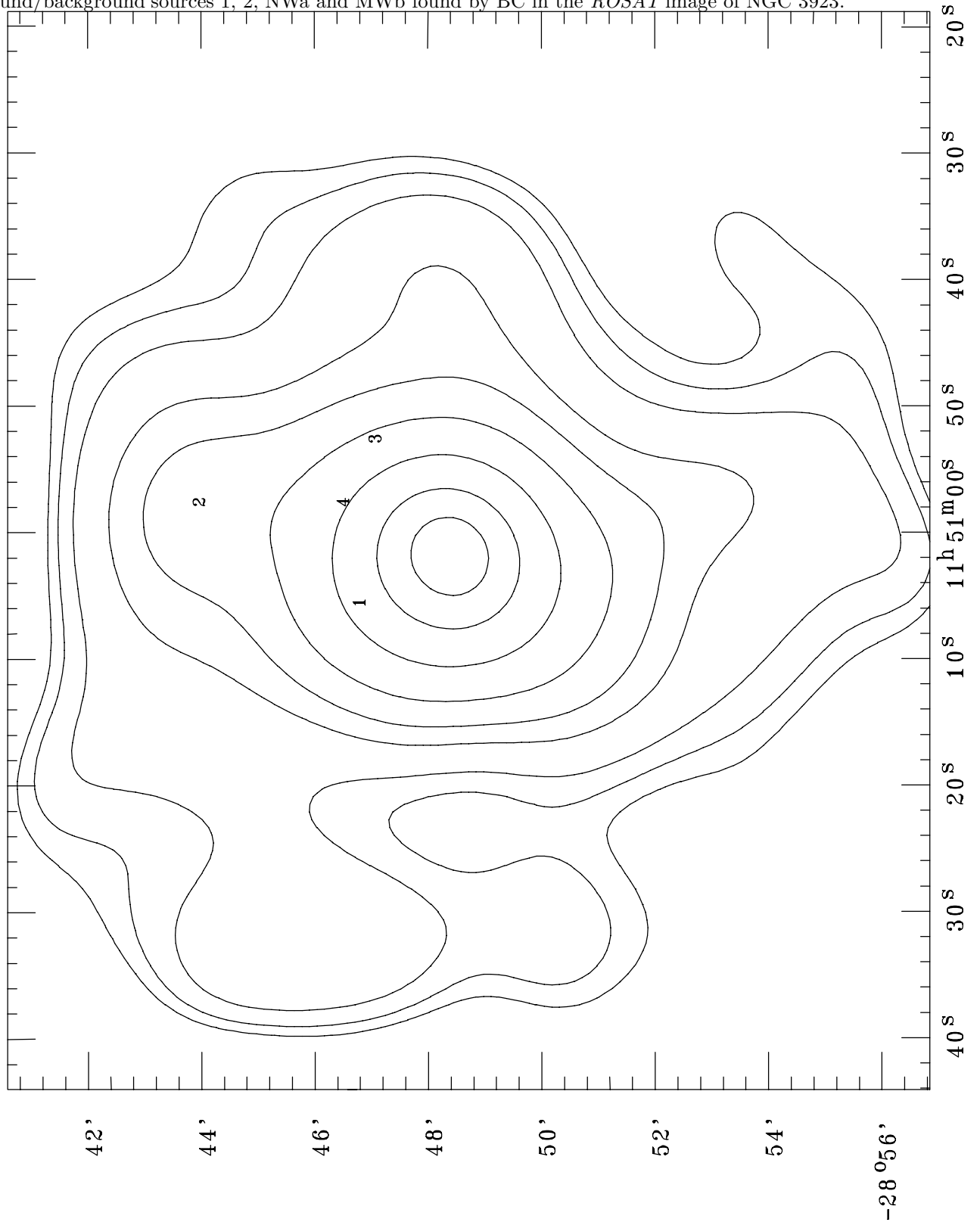


Table 2. Observation Log

Date	Exposure ^a (ks)		Count Rate ^b (ct/s)		Region ^c	
	LECS	MECS	LECS	MECS	LECS	MECS
1997 Jan 29	16.08	43.51	0.01±0.0015	0.01±0.0010	$R = 8'$	$a = 8', b = 6'$

^a On-source net exposure time. The LECS exposure time is considerably reduced with respect to the MECS one, because the LECS can operate only when the spacecraft is not illuminated by the Sun.

^b Background subtracted source count rates, with photon counting statistics errors, within the regions specified in the last column.

^c The extraction region is a circle for the LECS data and an ellipse of semi-axes a and b for the MECS data.

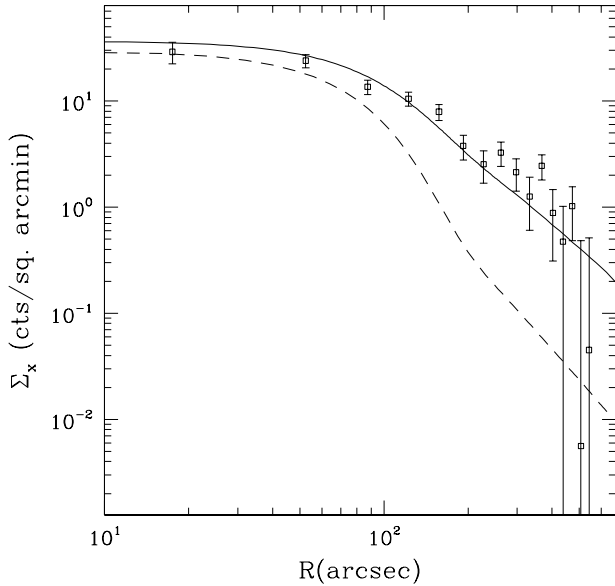


Fig. 2. Background subtracted azimuthally averaged surface brightness profile obtained from the MECS data over 1.7 – 10 keV). Also plotted is the PSF of the MECS for $E = 5$ keV (dashed line), and the convolution of the optical profile with the MECS PSFs calculated at the source photon energies (solid line; see Sect. 4.1). One pixel size is $8''$.

surface brightness profile of Fig. 2. Further implications coming from the presence of these sources for the spectral analysis are discussed in Sect. 4.

3.2. Spectral Analysis

Within the source regions determined as described above, we obtained the net count rates given in Table 2, and finally extracted the LECS and MECS spectra. Spectral channels covering the energy ranges 0.3–10 keV, and 1.7–10 keV respectively for the LECS and MECS have been used. The original channels have been grouped into larger bins, adequately filled for applicability of the χ^2 statis-

tic to assess the goodness of a fit (Cash 1979). The data have been compared to models, convolved with the instrumental and mirror responses, using the χ^2 minimization method. The spectral response matrices released in September 1997 have been used in the fitting process. We fitted the models simultaneously to the LECS and MECS spectral data.

Given the discussion of Sect. 1, the basic models used for the fits are the bremsstrahlung model, and two models describing the thermal emission of an optically thin hot plasma, both from continuum and lines: the standard Raymond-Smith model (hereafter R-S, Raymond & Smith 1977), and the MEKAL model. The latter is a modification of the original MEKA model (Kaastra & Mewe 1993) where the Fe-L shell transitions have been recalculated recently according to the prescriptions of Liedahl et al. (1995). The abundance ratios of the heavy elements cannot be constrained by the modeling, because of the poor statistics. So, we assume that the abundance ratios are solar, as accurately determined by Matsushita et al. (1998) for the ISM of the X-ray bright galaxy NGC 4636, using a very long *ASCA* exposure. The solar abundances are those given by Feldman (1992; e.g., the abundance of iron relative to hydrogen is $3.24 \cdot 10^{-5}$ by number, also known as meteoritic abundance). The models are modified by photoelectric absorption of the X-ray photons due to intervening cold gas along the line of sight, of column density N_H ; we take absorption cross sections according to Balucińska-Church & McCammon (1992). The results of the spectral analysis are presented in Tables 3 and 4.

3.2.1. One-component models

We first tried to fit one-component models to the data (Table 3). The probabilities of exceeding the reduced χ^2_{\min} are quite low (they range from 0.1 to 0.2) but the fits are formally acceptable. At the best fit N_H tends to be lower than the Galactic value; the fits are not worsened significantly when keeping N_H fixed at the Galactic value. All the one-component models give fits of comparable quality, and a temperature around 3 keV. The abundance at the

Table 3. One-component spectral fits

Model	$10^{-20}N_{\text{H}}^a$ (cm^{-2})	kT (keV)	Z (Z_{\odot})	χ^2	ν^b	χ^2/ν
Bremsstrahlung	1.	2.9 (2.0–5.4)		29.1	24	1.2
	6.4	3.1 (2.0–5.3)		33.1	25	1.3
R-S	1.	3.2 (2.1–5.4)	0. (0.–1.8)	28.9	23	1.3
	1.	3.0 (2.2–4.4)	1.0 (fixed)	30.2	24	1.3
	6.4	3.4 (2.0–5.4)	0.02 (0.–2.2)	33.0	24	1.4
	6.4	3.0 (2.1–4.3)	1.0 (fixed)	34.0	25	1.4
MEKAL	1.	3.2 (2.1–5.3)	0.07 (0.–1.8)	29.0	23	1.3
	1.	3.1 (2.2–4.0)	1.0 (fixed)	30.1	24	1.3
	6.4	3.4 (2.0–5.4)	0.05 (0–2.6)	33.2	24	1.4
	6.4	3.0 (2.1–4.3)	1.0 (fixed)	33.9	25	1.4
Cooling flow ^c	1.	5.7 (3.4–9.6)	0.45 (> 0.02)	21.6	23	0.9
	1.	4.7 (2.9–7.5)	1.0 (fixed)	22.3	24	0.9
	6.4	4.6 (2.9–7.5)	0.60 (> 0.05)	24.8	24	1.0
	6.4	4.6 (2.9–7.5)	1.0 (fixed)	25.0	25	1.0

^a When in this column $N_{\text{H}} = 6.4 \times 10^{20} \text{ cm}^{-2}$, it has been kept at this value (the Galactic one) during the fit. When N_{H} is a free parameter of the fit, it is constrained to lie in the interval $10^{20} - 10^{21} \text{ cm}^{-2}$, and its "best fit" value always turns out to be the lower boundary of the interval.

^b Number of degrees of freedom in the fit.

^c In this case kT in the third column gives the maximum temperature from which the gas is cooling.

The ranges of values between parentheses indicate the 90% confidence range of variation for one interesting parameter.

Table 4. Two-component spectral fits

best fit is extremely low, both for the MEKAL and the R-S models, but it is just constrained to be $< (2-3) Z_{\odot}$ by the data. So, we have also performed some fits with the abundance fixed at the solar value. These findings are in partial agreement with those obtained from *ASCA*-SIS data over (0.5–5) keV by BF: when keeping N_{H} fixed at the Galactic value, the single-component MEKAL fit gives them an abundance $Z = 0.07 Z_{\odot}$ close to that found by us, but a temperature of only $kT = 0.64$ keV. This could reflect the different extraction regions used for the spectrum, if the emission is much softer at the center; or could be the result of different spectral sensitivities between the *BeppoSAX*-MECS and the *ASCA*-SIS, from which the best data come in the cases of the two satellites. The spectral models derived from *ASCA* data are mostly constrained by the SIS data near 1 keV (BF), while those derived from *BeppoSAX* are mostly constrained by the MECS data at energies above that region.

3.2.2. Multi-component models

We then tried to fit multi-temperature models, to check whether the quality of the fits can be improved. Since

the R-S model gives results substantially equal to those given by the MEKAL model, for these data, we give in the following only the results obtained by using the more updated MEKAL model.

First we tried the fit with a cooling flow model, in which the cooling is isobaric, and the emissivity is as described in Johnstone et al. (1992); this model is made by the superposition of many thermal components, each described by a MEKAL model at a certain temperature. The results are given in Table 3; the fits are improved (the associated probability is 0.4–0.5). The upper temperature from which the gas cools is very high, ~ 4.7 keV; this is also the temperature at which the emission measure peaks (the emission-weighted temperature is somewhat lower). This modeling reveals that hard emission is present at a significant level, so that the distribution of the temperatures is forced to extend to high values ("high" for the temperatures expected in a galaxy cooling flow). The upper temperature values found here are higher than that given by BF ($kT_{\text{max}} = 1.13$ keV) for a fit with the same model, with N_{H} fixed at the Galactic value, and $Z = 0.11 Z_{\odot}$ resulting from the fit. The reasons for this discrepancy are likely the same given above for the one-component case.

In agreement with BF we find that the abundance at the best fit ($0.6 Z_{\odot}$) is raised with respect to that obtained from the one component MEKAL fit.

Then we tried the coupling of two thermal components (MEKAL+bremsstrahlung, and MEKAL+MEKAL) with the same N_H (Table 4). The quality of the fits is much improved now, and the probability of exceeding χ^2_{\min} is very large (> 0.9). As before, allowing N_H to be free does not significantly improve the fits; when Z is fixed at $1 Z_{\odot}$, N_H at the best fit is reasonably close to the Galactic value. In Fig. 3 we show the LECS and MECS data together with the two-component model which gives the best fit. More in detail, the results obtained by fitting with two thermal components are as follows:

a) MEKAL + bremsstrahlung models: the first turns out to describe a soft component, of temperature $kT_s \approx 0.4$ keV, and the second describes a hard component of temperature kT_h between 6.2 and 7.6 keV. kT_h is higher for a lower metallicity of the soft component. The abundance of the soft component is again very subsolar at the best fit ($0.16 Z_{\odot}$), and not constrained by the data.

b) Two MEKAL components: the results are similar. The abundance of the hard component turns out to be practically zero at the best fit; that of the soft component is also very low ($0.1 Z_{\odot}$), but again Z is just constrained to be > 0 . At the best fit the temperatures are kT_s around 0.4 keV and kT_h around 5 or 8 keV, depending on the abundance, fixed at the solar value or allowed to vary freely respectively. As before the temperature of the hard component is higher for a lower metallicity, but the effect is more pronounced now. In this kind of fit BF find temperatures close to ours ($kT_s = 0.55$ keV, and $kT_h = 4.2$ keV), but $Z = 2.0 Z_{\odot}$ ($> 0.1 Z_{\odot}$ at 90% confidence), with N_H kept at the Galactic value³.

Summarizing, all the two-component models give kT_s around 0.4 keV, and kT_h around 6–8 keV, except when the hard component is described by a MEKAL model with solar abundance (then $kT_h \approx 5$ keV). The latter case is also the one giving the worst fit among all the two-component models ($P = 0.85$). Heavy element abundances at the best fit tend to be very subsolar, except for the cooling flow model. The effect of imposing an abundance higher than that at the best fit is to produce a lower temperature of the hard component. This effect is particularly pronounced when fitting with two components (respectively kT_h decreases of ~ 1.5 to ~ 3 keV, using the bremsstrahlung and the MEKAL model for the hard component).

³ As for the previous two-component fits, the first best fit value of the abundance given by XSPEC is around solar, but an accurate exploration of the parameter space finds the true minimum χ^2 at a much lower abundance value. This behavior is somewhat opposite to that found by BF when fitting the *ASCA*-SIS data, which could be explained by the lower spectral sensitivity around 1 keV of the *BeppoSAX*-LECS.

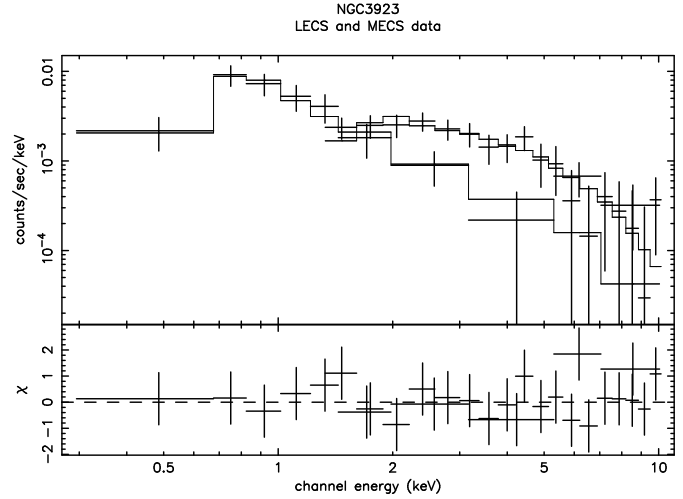


Fig. 3. The LECS and MECS spectral data with the best fit MEKAL + bremsstrahlung model with solar abundance and N_H fixed at the Galactic value, shown with thinner lines, and the residuals from the fit.

3.3. X-ray Fluxes and Luminosities

In Table 4 the absorbed fluxes in the (0.5–4.5) and (0.5–10) keV bands are given; unabsorbed fluxes are about 30% higher for the soft component, and 5 to 9% higher for the hard one, depending on the band. An average best fit value of the total absorbed flux $F(0.5 - 4.5 \text{ keV})$ is $\sim 8 \times 10^{-13} \text{ erg cm}^{-2} \text{ s}^{-1}$, and $F(0.5 - 10 \text{ keV}) \sim 10^{-12} \text{ erg cm}^{-2} \text{ s}^{-1}$. The ratio between the absorbed fluxes in the soft and in the hard components in the (0.5–4.5) keV band is ~ 0.93 , close to the value of 0.99 found by BF in the (0.5–5) keV band. This ratio actually is ~ 0.8 when Z is kept at $1 Z_{\odot}$ (and $kT_h \sim 6$ keV), and ~ 1.1 when $Z \sim 0$ ($kT_h \sim 8$ keV). An average value for the ratio between the absorbed fluxes in the soft and in the hard component in the (0.5–10) keV band is ~ 0.61 . Again it is lower (i.e., ~ 0.5) when Z is kept at $1 Z_{\odot}$, and higher (~ 0.7) when Z is very subsolar. In the (0.5–4.5) keV band, the soft component unabsorbed flux is 52% of the total, while the hard component amounts to $\sim 57\%$ of the total (0.5–10) keV unabsorbed flux.

Adopting the distance in Table 1, the fluxes can be converted into the following values of the luminosities in the (0.5–4.5) keV band: an average value of the soft component absorbed luminosity is $L_X = 7.8 \times 10^{40} \text{ erg s}^{-1}$ (unabsorbed $L_X = 1.0 \times 10^{41} \text{ erg s}^{-1}$), and of the hard component is $L_X = 8.2 \times 10^{40} \text{ erg s}^{-1}$ (unabsorbed $L_X = 8.9 \times 10^{40} \text{ erg s}^{-1}$).

4. Discussion

4.1. Origin of the X-ray emission in NGC 3923

The spectral analysis over the (0.5–10) keV band showed that the superposition of two thermal components of

$kT_s \approx 0.4$ keV, and $kT_h \approx 6 - 8$ keV, is the most reasonable representation of the spectral data. Whether the softer component is actually a multi-temperature component, such as a cooling flow, cannot be investigated with these data. Another caveat concerns the hard component, because, as seen in Sect. 3.1, BC detected a few point sources over the *ROSAT* PSPC image of NGC 3923. Were all these sources background AGNs, they could harden the spectrum of NGC 3923, and alter the estimate of the hard flux from NGC 3923. Given the number counts involved (see Sect. 3.1), the effects on the derived spectral parameters are expected to be within their uncertainties; in particular, there could be a spurious increase in the hard flux of $\lesssim 14\%$.

The value of kT_s suggests as origin of the soft emission a hot gas, that comes from the accumulation of the stellar mass loss during the galaxy lifetime. The value of kT_h is close to that found for the hard emission of the low L_X/L_B galaxy NGC 4382, based on *ASCA* data (i.e., ~ 6 keV; Kim et al. 1996). Following Fabbiano et al. (1992, 1994), these authors suggest for the origin of the hard component the integrated emission of LMXBs, an interpretation similar to that given for the X-ray emission of the bulges of early-type spirals (see Sect. 1). In fact the spectra of LMXBs can be described by a thermal bremsstrahlung model with $kT \sim 5$ keV (van Paradijs 1998), the spectrum of M31 can be fitted by bremsstrahlung emission at a temperature $kT > 3$ keV (Fabbiano et al. 1987), and those of bulge-dominated spirals can be fitted with bremsstrahlung at $kT \gtrsim 5$ keV (Makishima et al. 1989). We now examine more in detail the suggested origins for the two components of the X-ray emission of NGC 3923.

4.1.1. Origin of the soft component

How does kT_s compare with the possible average temperature of a gas flow in NGC 3923? A simple estimate of the kinetic temperature of the stars in NGC 3923 gives $kT = \mu m_p \sigma^2 = 0.36$ keV, when using the central stellar velocity dispersion in Table 1, and $\mu = 0.6$. This is close to kT_s found by the modeling, i.e., $kT_s = 0.39 - 0.45$ keV, with some room left for other heating mechanisms in addition to the thermalization of the stellar random motions. These are especially needed when considering that 0.36 keV is the *central* temperature of the stars, and that this decreases outward, while kT_s would be the emission-weighted temperature of the hot gas. Possible heating mechanisms are supernova heating (from type Ia supernovae, hereafter SNIa) and/or compressional heating operated by the gravitational field⁴. Compressional heating is produced when the hot ISM is in a global inflow. The

⁴ Compression can be operated also by an external medium, but this has not been observed around NGC 3923. Another more exotic possibility is Compton heating produced by accretion onto a supermassive black hole at the galaxy center (Ciotti & Ostriker 1997).

amount of the emission in the soft component ($\sim 10^{41}$ erg s^{-1}) is actually quite lower than that typical of a global inflow, in a galaxy of an optical luminosity as high as that of NGC 3923. For example, when $L_B \approx 2 \times 10^{11} L_\odot$, L_X of many times 10^{41} erg s^{-1} in the (0.5–4.0) keV band, and hot gas masses⁵ of a few times $10^{10} M_\odot$, are predicted by the steady state cooling flow models, for various combinations of dark matter and SNIa rates (e.g., Sarazin & White 1987, Bertin & Toniazzi 1995). Besides eliminating SNIa's, various kinds of reductions of the high L_X values in the framework of the cooling flow scenario have been suggested: by assuming, at fixed L_B , reductions in the stellar mass loss rate, or in the efficiency of its thermalization, or a higher efficiency of thermal instabilities in the hot gas (Sarazin & Ashe 1989, Bertin & Toniazzi 1995), or by including the effect of the rotation of the galaxy (Brighenti & Mathews 1996), or of a lower abundance (Irwin & Sarazin 1998). None of these effects has proved to be able to reduce L_X by a large factor. L_X up to 10^{41} erg s^{-1} , and gas temperatures higher than the stellar kinetic temperatures, are instead predicted for a galaxy like NGC 3923 from a gas that is experiencing an outflow or a partial wind; these can be driven by SNIa explosions at a rate comparable to the most recent optical estimates of Cappellaro et al. (1997) (Pellegrini & Fabbiano 1994, Pellegrini & Ciotti 1998). In addition, within this framework, global energy considerations and two-dimensional simulations showed that in general the flattening of the galaxy favors the loss of gas, while rotation has a minor role (Ciotti & Pellegrini 1996; D'Ercole & Ciotti 1998). This could be an explanation for the absence of a global inflow in NGC 3923, which is a considerably flat galaxy with no rotation (Sect. 2). A detailed modeling of the structure of NGC 3923, and hydrodynamical simulations of the hot gas behavior specific for this galaxy, are required for a definite answer about the gas flow state. There is a potential problem with a scenario that involves a substantial heating from SNIa's. The abundance of the soft component is not constrained by the *BeppoSAX* data for NGC 3923, but is extremely low at the best fit. Low abundances for the hot gas are not expected in presence of SNIa explosions, yet they have almost always resulted also from the analysis of *ASCA* data; there seems even to be a trend of decreasing abundances with decreasing L_X/L_B (Matsushita 1998). An unsolved puzzle is represented at present by the discrepancy between the low hot gas abundances and

⁵ The precise amount of hot gas can be calculated when the emissivity profile is known (i.e. in the hypothesis of spherical symmetry, $\epsilon(r) = \Lambda(T, Z) n(r)^2$, where r is the spatial radius, Λ is the cooling function and n the gas density), and this requires an accurate surface brightness profile, temperature profile, and abundance estimate, for the hot gas. Under the hypotheses of solar abundance, isothermality, and a standard β -model for the hot gas distribution (CFT), one has $M_{gas} = 5.0 \times 10^9 \sqrt{L_X/10^{41}} = 5.0 \times 10^9 M_\odot$ for NGC 3923. This is estimated to be accurate to factors of 2–4.

the abundances in the stellar mass loss which feeds the gas (but this discrepancy is narrowing for an increasing number of galaxies, after accurate re-analyses; Matsushita 1998, BF, Buote 1998), eventually further increased by the metals in the ejecta of SNIa's, which are seen to explode in E/SOs. Various solutions have been suggested (Arimoto et al. 1997, Fujita et al. 1996), but none has been recognized as the final one yet. We note that in NGC 3923 the stellar central iron abundance is $[\text{Fe}/\text{H}]=0.2$, or 1.6 solar, and that the mean abundance is likely a factor of 2 lower (the central Mg_2 value, from Faber et al. 1989, has been converted into central and average stellar iron abundance following the detailed prescriptions of Arimoto et al. 1997). If we adopt the abundance value of $Z = 2.0 Z_\odot$ for the hot gas found by BF (Section 3.2.2), in this galaxy there is room for enrichment by SNIa's exploding at the rate of Cappellaro et al. (1997).

Another possibility to explain the gas mass content of NGC 3923 is that a substantial amount of hot ISM was lost as a consequence of the episod of interaction or merger which is at the origin of the system of shells shown in the optical. Actually, the very detailed modeling of the shell formation that has been made for this galaxy, plus observations of the galaxy colors and ISM content at other wavelengths (see Sect. 2), established that the interaction or merger involved a small galaxy, devoid of gas, and that significative star formation (in the form of a starburst with supernova explosions that could have heated the gas) did not take place. It could be, though, that the gas flow is very sensitive to perturbations in the potential, and that even small perturbations can help a significant portion of the hot ISM to escape the galaxy. Numerical simulations are needed to test whether this was the case for NGC 3923.

4.1.2. Origin of the hard component

kT_h is in good agreement with that of bulge-dominated spirals; what about the amount of the hard emission in NGC 3923? CFT had estimated the luminosity of the integrated contribution of LMXBs in the (0.5–4.5) keV band (L_{dscr}) by scaling it from the emission of the bulge of M31. By assuming a linear relation with L_B , they had obtained $\log L_{dscr} = 29.6 + \log L_B$, where L_B is in L_\odot , and had estimated L_{dscr} for any given galaxy to scatter by about a factor of 3 about this relation, since this is the observed scatter in the X-ray to optical luminosity ratio for subclasses of spiral galaxies. This relation has been recently confirmed (both in shape and normalization) using *ASCA* data by Matsumoto et al. (1997). The present analysis gives, in the (0.5–4.5) keV band, $\log (L_{X,hard}/L_B) \approx 29.65$, i.e., $L_{X,hard}$ is close to the value predicted for L_{dscr} by CFT (it is just 12% higher, so well within the quoted uncertainties). An interpretation in terms of stellar sources of the hard emission can be judged also by inspecting Fig. 2, where the MECS surface brightness profile is compared with the distribution of optical light. The V-band profile

of NGC 3923 has been derived from Kodaira et al. (1990); since this extends out to a radius of $262''$, it has been extrapolated out to the radius of the X-ray emission with a fit. The optical profile has then been convolved with the MECS response, appropriate for the distribution of the counts in the different energy channels. A good agreement between the profile over (1.7–10) keV and the convolved optical profile is found, which would support the hypothesis of the origin of the hard emission in stellar sources. We note here that, consistently with the finding of an amount of hard emission 12% larger than the predicted L_{dscr} , and with the estimate of a possible spurious contribution up to 14% of the MECS counts from hard foreground/background sources, some excess of hard emission is also shown by the X-ray profile, with respect to the convolved stellar profile, at radii $\gtrsim 260''$, i.e., for $R > 5R_e$ (the excess at $260''$ is likely due to a foreground/background source, see Sect. 3.1). We cannot give a great significance to the detailed shape of the X-ray profile, because of the MECS moderate spatial resolution (Sect. 1); we just note that this hard excess cannot be produced by hot gas, neither belonging to the galaxy (at $kT_s=0.4$ keV), nor to a possible intragroup medium, because the low value of the velocity dispersion of the group (Sect. 2) corresponds to a kinetic temperature that is even lower than kT_s . An X-ray profile of NGC 3923 with a superior spatial resolution has been derived in the soft *ROSAT* band (0.4–2) keV by BC. For radii $> 10''$ this is in good agreement with the de Vaucouleurs extrapolation of the R-band profile within $103''$, while it is flatter than the optical one for radii $< 10''$. BC conclude that not all the hard emission is to be attributed to stellar sources, while some fraction of it could come from another phase of the hot gas. In line with the modeling done to interpret the *ROSAT* data of another galaxy which showed an X-ray profile centrally flatter than the optical one (NGC 4365; Pellegrini & Fabbiano 1994), we suggest the possibility that the hot gas has quite an extended distribution in the central regions, i.e., flatter than the optical one within 10 arcsec (consistently with what can be derived also by the *BeppoSAX* data, BC estimate that just 35% of the total 0.4–2 keV emission is due to a hard component; so this cannot fully determine the total shape). The hypothesis of some peculiarities in the hot gas distribution can be supported also by the consideration of the past galaxy history, where a merging occurred.

4.2. The nature of the X-ray emission in medium and low L_X/L_B galaxies

A fundamental diagnostic of the X-ray emission from early-type galaxies is the L_X-L_B plane. The large scatter in L_X of more than two orders of magnitude at fixed L_B shown by this plane is not an artifact of distance errors [see Pellegrini & Ciotti (1998) for a more detailed discussion]. The explanation of this scatter is a largely varying quantity of hot gas within the galaxies (e.g., Mat-

sumoto et al. 1997), but it is still a controversial issue how these variations are established. Are they fundamentally a consequence of environmental differences, or of different dynamical phases for the hot gas flows (provided that it was not possible to reproduce the observed scatter with various adjustments to the cooling flow scenario, see Sect. 4.1.1)? The first hypothesis can affect only galaxies in clusters or groups; actually this is the case for the majority of E/S0s. Then accretion of external gas can explain the extremely X-ray bright objects (Renzini et al. 1993, Mathews & Brighenti 1998), while in the X-ray faint ones the hot gaseous halos should have been stripped by ambient gas, if it is sufficiently dense, or in encounters with other galaxies (White & Sarazin 1991). It is not clear yet whether the primary stripping agents would be other galaxies or the ambient gas. The effectiveness of the stripping by an ambient gas has been explored theoretically, and it turned out to depend largely on various factors (shape of the orbit, velocity and internal dynamics of the galaxy, density of the environment), for which the observed range is wide (e.g., Portnoy et al. 1993). Observationally, evidence of stripping by the intracluster medium is the famous plume shown by the hot halo of the Virgo elliptical M86. *ROSAT* though showed that the sample of early-type galaxies of the Coma cluster, that is richer than Virgo, has the same average L_X/L_B as that of Virgo (Dow & White 1995); but that instead the X-ray luminosities are on average lower in the rich cluster A2634 (Sakelliou & Merrifield 1998). In the Pegasus I group and in the poor cluster Cancer A, where a medium has been detected, the X-ray image shows also many clumps that could be the X-ray halos from individual galaxies with a ‘normal’ L_X/L_B (Trinchieri et al. 1997). For what is concerning the interactions among galaxies, observationally there is an indication that lower L_X/L_B galaxies occur across the whole range of galaxy densities, while the higher L_X/L_B ones are mostly confined at low densities (Mackie & Fabbiano 1997). Theoretically, galaxy interactions could produce some scatter in L_X/L_B as follows: group-dominant ellipticals may acquire dark matter and hot gas by mergers or tidal interactions early in their evolution, and then become very X-ray bright; the other E/S0s, in which the gas is in a global inflow, may be tidally truncated in their dark matter and hot gas halo, at different radii, and so end up with different sizes and different L_X/L_B (Mathews & Brighenti 1998). The problems with explaining the L_X/L_B plane only with environmental factors are that: 1) low or medium L_X/L_B values are also shown by galaxies that do not reside in a high density medium [e.g., NGC 5866 (Pellegrini 1994), NGC 3923], and by galaxies that reside in a region where the galaxy density is not particularly high, and where also galaxies of high L_X/L_B are found (Mackie & Fabbiano 1997); 2) the effect of merging and tidal interaction on the hot gas flow (in various dynamical states) is still quite conjectural, as is the evolution of the hot gas in galaxies that undergo these phenom-

ena. The only models available so far, those of Mathews & Brighenti (1998), are not aimed at reproducing all the L_X/L_B variation, down to the lowest L_X/L_B values observed ($\log L_X/L_B \sim -4$, with L_X and L_B in erg s^{-1}), but stop at $\log L_X/L_B \sim -2.8$. Probably it is not possible to reproduce the lowest L_X/L_B values by simply truncating global inflows, because one continues to obtain galaxies quite rich in hot gas. We note here also that NGC 3923 is a group-dominant elliptical, but does not show a very large hot gas content ($\log L_X/L_B \approx -3.3$).

The second way of explaining the scatter, through different dynamical phases of the gas flows, regulated by *internal* agents, has the advantage of being a *general* explanation, i.e., of applying to all the galaxies, regardless of their environment (accretion is always needed for the extremely X-ray bright galaxies). At fixed L_B , any of the flow phases ranging from winds to subsonic outflows to partial and global inflows, can be found at the present epoch, depending on the various depths and shapes of the potential well of the galaxies (Ciotti et al. 1991, Pellegrini & Ciotti 1998). In this way the large scatter in L_X is easily accounted for: in the X-ray bright galaxies the soft X-ray emitting gas dominates the emission, being in the inflow phase, that resembles a cooling flow; in the X-ray faint galaxies the hard stellar emission dominates, these being in the wind phase; in intermediate L_X/L_B galaxies, the hot gas is in the outflow or partial wind phase, and the amount of soft emission varies from being comparable to that of the stars, to being dominating. In this scenario a crucial role is played by the SNIa explosions, that heat the flow in an extent sometimes large enough to drive all or part of the gas out of the galaxies, and by the evolution of the explosion rate⁶. Numerical simulations using the updated rate given recently by Cappellaro et al. 1997, which is reduced with respect to that used by Ciotti et al. (1991), show that the partial wind phase is the most frequent, and that a large scatter in the stagnation radius corresponds to a large scatter in the amount of hot gas (Pellegrini & Ciotti 1998). The problem with this scenario is represented by the puzzle of the extremely low hot gas iron abundances revealed by *ASCA* (Sect. 4.1.1).

5. Conclusions

We have analysed the X-ray properties of the E4 galaxy NGC 3923 over the energy range (0.5–10) keV, using *BeppoSAX* data. Our findings are as follows.

1. The superposition of two thermal components of $kT_s \approx 0.4$ keV, and $kT_h \approx 6 - 8$ keV, is the most reasonable representation of the spectral data. The heavy element

⁶ The hot gas can be expelled from the galaxies also when a central massive black hole is present, because the gas flows are found to be unstable due to Compton heating (Ciotti & Ostriker 1997).

abundances cannot be constrained due to the uncertainties in the spectral data; at the best fit they are very subsolar (except for the cooling flow model), and much lower than the stellar mean abundance.

2. The two components have roughly comparable fluxes in the (0.5–4.5) keV band, while the hard component amounts to $\sim 3/5$ of the total (0.5–10) keV flux.
3. The temperature of the softer component suggests as its origin the emission of a hot gas, the origin of the hard component is likely the integrated emission of LMXBs. In fact, in addition to the spectral shape, also the amount of the hard emission is consistent with that predicted for stellar sources in NGC 3923.
4. kT_s is close to the kinetic temperature of the stars in NGC 3923, but some additional heating is needed. Since L_X is less than predicted by a steady state cooling flow model, for a galaxy of an optical luminosity as high as that of NGC 3923, it is suggested that a large fraction of the stellar mass loss was removed by internal agents, such as the heating of SNIa's explosions, and that this process was helped by the flat mass distribution of the galaxy. Another possibility, that has to be explored with numerical simulations, is that a substantial amount of hot gas was lost as a consequence of the episod of interaction or merger, with a much smaller galaxy, which gave origin to the system of shells visible in the optical.
5. The origin of the X-ray emission in galaxies of low and medium L_X/L_B is finally reviewed. The detailed study of these galaxies is crucial to establish which factor plays the major role in lowering the amount of hot gas, and so to explain the large scatter in the L_X/L_B plane. Is this factor to be linked to external agents, as stripping by ambient gas or interactions with other galaxies, or to internal heating mechanisms, such as SNIa explosions or accreting supermassive black holes? The galaxy discussed here is not surrounded by a dense medium, so that ram pressure stripping cannot be invoked; but galaxy interactions clearly took place, and so cannot be excluded as causes of the loss of hot gas. In general, since many other low and medium L_X/L_B galaxies reside in small groups, in which the density of the environment is presumably low or very low, it is concluded that the most effective mechanism, in order to explain the L_X/L_B of these galaxies always with environmental effects, must be galaxy interactions. But it is remarked that in general low or medium L_X/L_B values are also shown by galaxies that reside in a region where the galaxy density is not particularly high, and where also galaxies of high L_X/L_B are found.
6. Another result emerged here is that NGC 3923 is the dominant elliptical of its group, but has just a medium value of L_X/L_B . So, an optically dominant galaxy does not always have a high hot gas content.

NGC 3923 also belongs to a program of investigating the nature of the X-ray emission in flat galaxies with very well known internal kinematics and photometry (see Pellegrini et al. 1997), for which the mass profile can be derived with accuracy. Two-dimensional numerical simulations are in program to study in detail the hot gas evolution in these galaxies, including the effect of galaxy interactions for this particular case.

Acknowledgements. This research has made use of SAXDAS linearized and cleaned event files (rev0) produced at the BeppoSAX Science Data Center. F. Fiore is warmly thanked for enlightenments concerning SAX instrumental properties and data analysis. Stimulating discussions with F. Brighenti, L. Ciotti, A. D'Ercole and G. Trinchieri are acknowledged. The referee, D. Buote, is also thanked for comments that improved the paper.

References

- Arimoto N., Matsushita K., Ishimaru Y., Ohashi T., & Renzini A., 1997, *ApJ* 477, 128
- Balucińska-Church M., McCammon D., 1992, *ApJ* 400, 699
- Bertin G., Toniazzo T., 1995, *ApJ* 451, 111
- Boella G., et al., 1997a, *A&AS* 122, 299
- Boella G., et al., 1997b, *A&AS* 122, 327
- Brighenti F., Mathews W., 1996, *ApJ* 470, 747
- Buote D., 1998, submitted to *MNRAS* (astro-ph/9811080)
- Buote D., Canizares C.R., 1998, *MNRAS* 298, 811 (BC)
- Buote D., Fabian A.C., 1998, *MNRAS* 296, 977 (BF)
- Canizares C.R., Fabbiano G., Trinchieri G., 1987, *ApJ* 312, 503 (CFT)
- Cappellaro E., Turatto M., Tsvetkov D.Y., O.S. Bartunov, C. Pollas, R. Evans, M. Hamuy, 1997, *A&A* 322, 431
- Carter D., Thomson R.C., Hau G.K.T., 1998, *MNRAS* 294, 182
- Cash W., 1979, *ApJ* 228, 939
- Ciotti L., D'Ercole A., Pellegrini S., Renzini A., 1991, *ApJ* 376, 380
- Ciotti L., Pellegrini S., 1996, *MNRAS* 279, 240
- Ciotti L., Ostriker J.P.O., 1997, *ApJ* 487, L105
- Colbert E.J.M., Mushotzky R.F., 1998, in: Proc. of the 32nd COSPAR Session E1.2 (1998 July 15-17 Nagoya) "The AGN-Normal Galaxy Connection"
- de Vaucouleurs G., de Vaucouleurs A., Corwin Jr. H.G., Buta R.J., Paturel G., Fouque P., 1991, *Third Reference Catalogue of Bright Galaxies*. Springer Verlag, New York.
- Dow K.L., White S.D.M., 1995, *ApJ* 439, 113
- Fabbiano G., Trinchieri G., Van Speybroeck L., 1987, *ApJ* 316, 127
- Fabbiano G., 1989, *Ann. Rev. Astr. Ap.* 27, 87
- Fabbiano G., Kim D.W., Trinchieri G., 1992, *ApJS* 80, 531
- Fabbiano G., Kim D.W., Trinchieri G., 1994, *ApJ* 429, 94
- Faber S.M., et al., 1989, *ApJS* 69, 763
- Feldman U., 1992, *Physica Scripta* 46, 202
- Forbes D.A., 1991, *MNRAS*, 249, 779
- Forman W., Jones C., Tucker W., 1985, *ApJ* 293, 102
- Franx M., Illingworth G., Heckman T., 1989, *ApJ*, 344, 613
- Fujita Y., Fukumoto J., Okoshi K., 1996, *ApJ* 470, 762
- Garcia, A.M. 1993, *A&AS* 100, 47
- Giacconi, R., et al. 1979, *ApJ* 230, 540

- Huchra J., Geller M., 1982, *ApJ* 257, 423
- Irwin J.A., Sarazin C.L., 1998, *ApJ* 499, 650
- Johnstone, R.M., Fabian, A.C., Edge, A.C., Thomas, P.A. 1992, *MNRAS*, 255, 431
- Kaastra, J.S., and Mewe, R. 1993, *A&AS* 97, 443
- Kim, D.W., Fabbiano, G., Trinchieri, G. 1992, *ApJ* 393, 134
- Kim, D.W., Fabbiano, G., Matsumoto, H., Koyama, K., Trinchieri, G. 1996, *ApJ* 468, 175
- Kodaira, K., Okamura, S., and Ichikawa, S. 1990, *Photometric Atlas of Northern Bright Galaxies*, University of Tokyo Press.
- Liedahl, D.A., Osterheld, A.L., Goldstein, W.H. 1995, *ApJ* 438, L115
- Mackie G., Fabbiano G., 1997, in: M. Arnaboldi, G.S. Da Costa and P. Saha (eds.) *The Second Stromlo Symposium*, ASP Conf. Ser. 116, p. 401
- Makishima, K., et al. 1989, *PASJ* 41, 697.
- Mathews, W.G., and Brighenti, F. 1998, *ApJ* 503, L15
- Matsumoto, H., Koyama, K., Awaki, H., Tsuru, T., Loewenstein, M., Matsushita, K. 1997, *ApJ*, 482, 133
- Matsushita K., et al. 1994, *ApJ* 436, L41
- Matsushita K. 1998, *ISAS Research Note* 640 (PhD thesis)
- Matsushita, K., Makishima, K., Ikebe, Y., Rokutanda, E., Yamasaki, N., Ohashi, T. 1998, *ApJ* 499, 13
- McElroy, D.B. 1995, *ApJS* 100, 105
- Parmar, A.N., et al. 1997, *A&AS* 122, 309
- Pellegrini, S. 1994, *A&A*, 292, 395
- Pellegrini, S., and Fabbiano, G. 1994, *ApJ* 429, 105
- Pellegrini, S., Held, E.V., and Ciotti, L. 1997, *MNRAS*, 288, 1
- Pellegrini, S., and Ciotti, L. 1998, *A&A*, 333, 433
- Portnoy D., Pistinner S., Shaviv G., 1993, *ApJS* 86, 95
- Quinn, P. 1984, *ApJ*, 279, 596
- Raymond, J., and Smith, B.W. 1977, *ApJS* 35, 419
- Renzini A., Ciotti L., D'Ercole A., Pellegrini S. 1993, *ApJ* 419, 53
- Sakelliou I., Merrifield M.R., 1998, *MNRAS* 293, 489
- Sarazin, C.L., and White, R.E. 1987, *ApJ* 320, 32
- Sarazin, C. L., and Ashe, G. A. 1989, *ApJ* 345, 22
- Stark, A.A., Gammie, C.F., Wilson, R.W., Bally, J., Linke, R.A., Heiles, C., and Hurwitz, M. 1992, *ApJS* 79, 77
- Thomson, R.C. 1991 *MNRAS*, 253, 256
- van Paradijs J., 1998, in: R. Buccheri, J. van Paradijs, M.A. Alpar (eds.) *The Many Faces of Neutron Stars*. Kluwer Academic Publishers
- Trinchieri, G., Fabbiano, G., and Kim, D.W. 1997, *A&A* 318, 361
- White, R.E.III, and Sarazin, C.L. 1991, *ApJ* 367, 476

Table 4. Two-component spectral fits

Model1	Model2	$10^{-20} N_{\text{H}}^a$ (cm^{-2})	kT_1 (keV)	kT_2 (keV)	Z (Z_{\odot})	ν^b	χ^2/ν	F_1 (0.5-4.5 keV) ($10^{-13} \text{erg cm}^{-2} \text{s}^{-1}$)	F_2 (0.5-4.5 keV) ($10^{-13} \text{erg cm}^{-2} \text{s}^{-1}$)	F_1 (0.5-10 keV) ($10^{-13} \text{erg cm}^{-2} \text{s}^{-1}$)	F_2 (0.5-10 keV) ($10^{-13} \text{erg cm}^{-2} \text{s}^{-1}$)
R-S	Brems.	6.4	0.44 (0.27–0.71)	7.9 (> 3.6)	0.06 (> 0)	22	0.55	4.2 (0.1–15)	3.9 (2.8–5.7)	4.2 (0.1–15)	6.0 (4.4–9.0)
MEKAL	Brems.	10	0.40 (0.26–0.79)	7.5 (> 3.6)	0.08 (> 0)	21	0.58	4.4 (0.3–22)	3.8 (2.7–5.5)	4.4 (0.3–22)	6.0 (4.2–8.7)
		2.8	0.45 (0.25–0.75)	6.4 (> 3.3)	1.0 (fixed)	22	0.58	3.4 (1.4–11)	4.4 (3.3–6.2)	3.4 (1.4–11)	6.4 (4.9–9.1)
		6.4	0.44 (0.26–0.69)	7.6 (> 3.6)	0.16 (> 0)	22	0.56	4.2 (0.1–18)	3.9 (2.8–5.8)	4.2 (1.7–7.6)	6.1 (4.4–9.0)
		6.4	0.41 (0.26–0.67)	6.2 (3.7–20.0)	1.0 (fixed)	23	0.55	3.6 (1.7–7.6)	4.2 (3.2–5.8)	3.6 (1.7–7.6)	6.3 (4.7–8.9)
MEKAL	MEKAL	2.8	0.43 (0.24–0.80)	5.0 (> 2.8)	1.0 (fixed)	22	0.69	3.2 (1.6–11)	4.5 (3.3–6.0)	3.2 (1.6–11)	6.5 (4.8–8.7)
		6.4	0.43 (0.27–0.69)	7.8 (> 3.6)	0.10 ^c (> 0)	21	0.58	4.3 (0.1–15)	3.9 (2.8–5.7)	4.3 (0.1–15)	6.1 (4.3–8.9)
		6.4	0.39 (0.25–0.70)	4.8 (> 2.9)	1.0 (fixed)	23	0.66	3.4 (2.8–6.8)	4.4 (3.1–5.5)	3.4 (2.8–6.8)	6.3 (4.5–8.0)

^a The same as in the note *a* to Table 3, except that here, when N_H is a free parameter, in two cases a true best fit value is found, and in the third case the "best fit" value is actually the upper boundary of the interval allowed for the fitting.

^b number of degrees of freedom of the fit.

^c This is the abundance of the soft component; that of the hard component at the best fit is 0. (0.–1.6).

The ranges of values between parentheses indicate the 90% confidence limits on one interesting parameter.

The X-ray fluxes F in the (0.5–4.5) and (0.5–10) keV bands are absorbed.